The International Journal of Engineering and Science (IJES)
ISSN (e): 2319 – 1813 ISSN (p): 23-19 – 1805
|| Pages || PP 74-80 || 2020 ||

Stability analysis of MHD stagnation point flow and heat transfer over a shrinking sheet

GolamMortujaSarkar*[1], BikashSahoo[1]
[1]*Department of Mathematics, NIT Rourkela, Odisha, India*
**Corresponding author Email: 517ma1009@nitrkl.ac.in*

----------ABSTRACT----------
The MHD stagnation point flow and heat transfer over a linearly shrinking sheet has been considered in this article. The Navier-Stokes equations are transformed into a coupled set of non-linear ODEs using similarity variables, and then solved numerically. We have found that there exist two solution branches up to a particular value of the shrinking rate, treated as critical value. It is noticed that increasing in magnetic parameter (Hartmann number), increase the absolute value of the critical point. The effects of Hartmann number and shrinking parameter show opposite character in the velocity and thermal profiles for both the solution branches. To understand the flow phenomena, it's essential to determine the stable solution. Thus, we have carried a linear temporal stability analysis of these two solution branches to embed the physically stable solution.
KEYWORDS;-*Stagnation point flow, Dual solutions, Shooting technique, Stability analysis, Shrinking sheet.*

I. INTRODUCTION

Incompressible viscous boundary layer flows and heat transfer towards a shrinking/stretching sheet have generated considerable interest among researchers due to its immense industrial and practical applications, for example glass-fiber production, polymer extrusion, cooling of electronic devicesetc. The pioneer work was due to Crane [1], who studied the steady 2D boundary layer flow of a Newtonian fluid towards a linearly stretching surface and found the analytical solution. This problem was extended by many authors (Refs. [2], [3]) by considering different fluids and diverse physical effects. Another widely studied problem is the 2D stagnation point flow of a viscous fluid over a flat surface. This flow problem was initially introduced by Hiemenz [4]. Later, Chiam [5] combined the works of [1] and [4] that is the Hiemenz flow over a linearly stretching sheet. Motivated by Chiam's [5] work, many authors extended this problem by considering various physical aspects. One may refer the work of Mahapatra and Gupta [6] and the related references therein.

Literature survey indicates that the stagnation point flow due to shrinking sheet was reported by Wang [7]. He showed that two solution branches exist numerically within a limited range of the shrinking rate and no solution exists for higher shrinking rate. Furthermore, Bhattacharyya [8] extended Wang's [7] work by adding chemical reaction in his flow model. He reported that the thickness of the boundary layer in the upper solution branches (USB) is lower than the lower solution branches (LSB). Since then, many researchers worked with this model by considering various physical aspects and found dual solutions in the shrinking case only (see Ref. [9], [10]). In the case of dual solutions it becomes essential to carry a stability analysis to find the most feasible solution. Recently, Awaludin et al. [11] analyzed the stability of the dual solutions of Wang's [7] work and reported that USB is the stable solution.

In this article, we have studied the steady MHD stagnation point flow towards a stretching/shrinking surface with uniform surface temperature. Our prime motivation is to extend the two-dimensional study of Wang [7] in the presence of magnetic field with heat transfer and test the stability of the dual solution branches. The RK4 with shooting algorithm is employed to obtain the self-similar solution numerically.

II. FLOW ANALYSIS

We have considered the steady 2D stagnation point flow of an incompressible, electrically conducting viscous fluid impinging on a stretching/shrinking sheet at $y = 0$. A uniform magnetic field B_0 is imposed along the y axis. Let the velocity of the sheet be$U_w = bx$, where $b > or < 0$ according to the stretching or shrinking of the sheet. We also assume that the temperature of the stretching/shrinking sheet be T_w and the ambient fluid temperature be T_∞. Figs. 1 and Figs. 2 are depicted the schematic diagram of this flow model. The velocities of the potential flow are defined as

$$U = ax, \quad V = -ay \tag{1}$$

Where$a$ is constant. Let p_0 be the stagnation pressure and$p$ be the arbitrary point pressure. Using the Bernoulli's equation, the pressure distribution is as follow

$$p_0 - p = \frac{1}{2}\rho(U^2 + V^2) \quad (2)$$

Under this assumption the Navier-Stokes equations are as follow

$$u_x + v_y = 0 \quad (3)$$

$$uu_x + vu_y = U\frac{dU}{dx} + \nu u_{yy} - \frac{\sigma B_0^2}{\rho}(u - U) \quad (4)$$

$$uT_x + vT_y = \alpha T_{yy} \quad (5)$$

Where σ, ρ, α and ν are the electric conductivity, fluid density, thermal diffusivity and kinematic viscosity respectively. Here (u, v) represent the velocity components along (x, y) axes respectively.
The relevant no-slip boundary conditions (BCs) are

$$u = U_w, \quad v = 0, \quad T = T_w \text{ at } y = 0 \quad (6.1)$$

$$u \to U, \quad T \to T_\infty \text{ as } y \to \infty \quad (6.2)$$

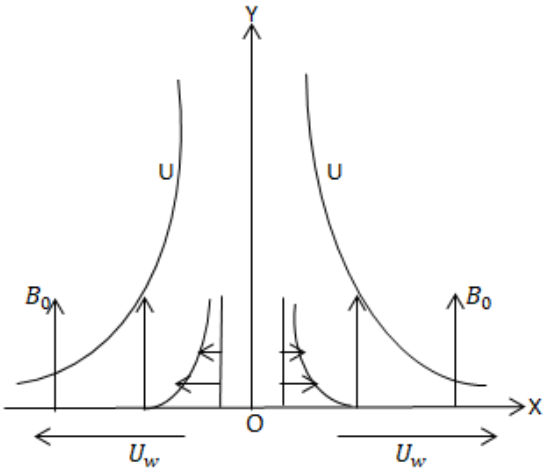

Fig. 1. Stretching sheet

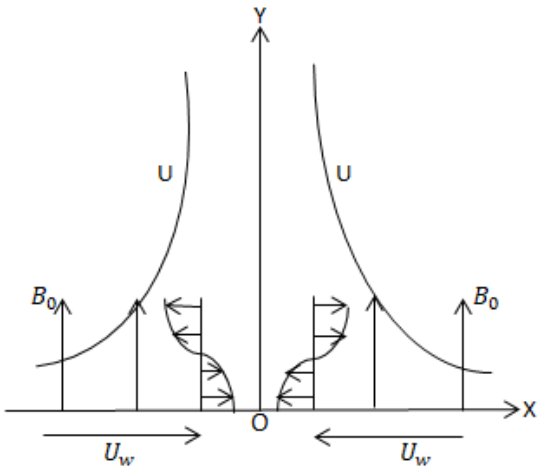

Fig. 2. Shrinking sheet

We use the following similarity variables

$$\psi = \sqrt{\nu x U}\varphi(\eta), \quad \theta = \frac{T - T_\infty}{T_w - T_\infty}, \quad \eta = \sqrt{\frac{U}{\nu x}}y \quad (7)$$

where,ψ is the stream function and $u = \psi_y, \quad v = -\psi_x$. Therefore, we obtain

$$u = ax\varphi'(\eta), \quad v = -\sqrt{a\nu}\varphi(\eta) \quad (8)$$

Substituting (7) and (8) into Eqs. (3)-(5) we get

$$\varphi''' + \varphi\varphi'' + \left(1 - \varphi'^2\right) + M^2(1 - \varphi') = 0 \quad (9)$$

$$\theta'' + \Pr\varphi\theta' = 0 \quad (10)$$

The boundary conditions (6.1) and (6.2) reduced to

$$\varphi(0) = 0, \quad \varphi'(0) = \lambda, \quad \theta(0) = 1 \quad (11.1)$$

where,$M = \sqrt{\frac{\sigma}{\rho a}}B_0$, $Pr = \frac{\nu}{\alpha}$, and $\lambda = \frac{b}{a}$ are the Hartmann number, Prandtl number and the velocity ratio respectively. The local skin friction coefficient (frictional drag coefficient) and local Nusselt number are defined by

$$\varphi'(\eta) \to 1, \quad \theta(\eta) \to 0 \quad \text{as} \eta \to \infty \quad (11.2)$$

$$C_\varphi = \frac{\mu(\frac{\partial u}{\partial y})_{y=0}}{\frac{1}{2}\rho U^2}, \quad Nu_x = -\frac{x(\frac{\partial T}{\partial y})_{y=0}}{T_w - T_\infty} \quad (12)$$

Now using the (7) and (8) into (12), we obtain

$$\varphi''(0) = 2Re_x^{1/2}C_\varphi, \quad -\theta'(0) = Re_x^{-1/2}Nu_x \quad (13)$$

where Re_x is the local Reynolds number.

III. NUMERICAL SOLUTIONS

The system of nonlinear similarity Eqs. (9) and (10) subject to BCs (11.1) and (11.2) are solved numerically. The BVP has been rewritten as a system of first order IVP. We guessed the values of $\varphi''(0)$ and $\theta'(0)$. Here we have used the shooting technique, which is a combination of RK4 and a zero finding algorithm. Then the computed values of $\varphi'(\eta)$ and θ(η) at $\eta = \infty$ are compared with the BCs $\varphi'(\eta_\infty) \to 1$ and $\theta(\eta_\infty) \to 0$. The value of η_∞ has been taken sufficiently large to ensure the far field BCs are satisfied asymptotically. The initial guesses $\varphi''(0)$ and $\theta'(0)$ are refined by the zero finding algorithm Newton-Raphson method. The C++ code was run on a personal computer. Interestingly dual solution branches are obtained numerically in the negative range of λ. To verify the efficiency of our numerical computations, we have compared our obtained values of $\varphi''(0)$ for both the solution branches at $M = 0$ with the reported results of Wang [7] and Bhattacharyya [8], which are presented in Table-1.

IV. STABILITY ANALYSIS

Sharma et al. [10] and Awaludin et al. [11] showed that the USB are the only stable solution by adopting the method of Merkin [12]. Similarly, we have carried a linear temporal stability analysis to embed the stable and feasible solution. We therefore consider the following unsteady form of Eqs. (4) and (5)

$$u_t + uu_x + vu_y = U\frac{dU}{dx} + \nu u_{yy} - \frac{\sigma B_0^2}{\rho}(u - U) \quad (14)$$

$$T_t + uT_x + vT_y = \alpha T_{yy} \quad (15)$$

We introduce the following new similarity variables

$$\psi = \sqrt{\nu x U}\varphi(\eta,\tau), \quad \theta(\eta,\tau) = \frac{T-T_\infty}{T_w - T_\infty}, \quad \eta = \sqrt{\frac{U}{\nu x}}y, \quad \tau = \left(\frac{U}{x}\right)t \quad (16)$$

where τ is new dimensionless time. Substituting (16) into Eqs. (14) and (15) we obtain

$$\varphi_{\eta\eta\eta} + \varphi\varphi_{\eta\eta} + \left(1 - \varphi_{\eta\eta}^2\right) + M^2(1 - \varphi_\eta) - \varphi_{\eta\tau} = 0 \quad (17)$$

$$\theta_{\eta\eta} + Pr\left(\varphi\theta_\eta - \theta_\tau\right) = 0 \quad (18)$$

The BCs in terms of new variables become,

$$\varphi(0,\tau) = 0, \quad \varphi_\eta(0,\tau) = \lambda, \quad \theta(0,\tau) = 1 \quad (19)$$

$$\varphi_\eta(\eta,\tau) \to 1, \quad \theta(\eta,\tau) \to 0 \text{ as } \eta \to \infty \quad (20)$$

Table 1. Comparison of the values of $\varphi''(0)$ for several λ at $M = 0$.

λ	Present study		Wang [7]		Bhattacharyya [8]	
	UB	LB	UB	LB	UB	LB
-0.25	1.4022408		1.40224		1.4022405	
-0.50	1.4956697		1.49567		1.4956697	
-0.75	1.4892982		1.48930		1.4892981	
-1.00	1.3288168	0	1.32882	0	1.3288169	0
-1.15	1.0822311	0.1167018	1.08223	0.116702	1.0822316	0.1167023
-1.20	0.9324733	0.2336497			0.9324728	0.2336491
-1.2465	0.5842916	0.5542858	0.55430		0.5842915	0.5542856
-1.24657	0.5745258	0.5639989			0.5745268	0.5639987

Here, we choose $\varphi(\eta) = \varphi_0(\eta)$ and $\theta(\eta) = \theta_0(\eta)$ to test the stability of steady solution. Further, following Sharma et al. [10] and Awaludin et al. [11] we take

$$\varphi(\eta,\tau) = \varphi_0(\eta) + e^{-\beta\tau}\tilde{\varphi}(\eta,\tau) \quad (21.1)$$

$$\theta(\eta,\tau) = \theta_0(\eta) + e^{-\beta\tau}\tilde{\theta}(\eta,\tau) \quad (21.2)$$

where β is the rate of disturbance and $\tilde{\varphi}$ and $\tilde{\theta}$ are small corresponding to the steady solutions $\varphi_0(\eta)$ and $\theta_0(\eta)$ respectively. The solution is stable if β is positive, and the solution is unstable if β is negative. Substituting (21.1) and (21.2) into (17-20), and after linearization we obtain

$$\tilde{\varphi}_{\eta\eta\eta} + \varphi_0\tilde{\varphi}_{\eta\eta} + \varphi_0''\tilde{\varphi} - (2\varphi_0' + M^2 - \beta)\tilde{\varphi}_\eta - \tilde{\varphi}_{\eta\tau} = 0 \quad (22)$$

$$\tilde{\theta}_{\eta\eta} + \mathrm{Pr}\left(\varphi_0\tilde{\theta}_\eta + \theta_0'\tilde{\varphi} + \beta\tilde{\theta}\right) - \tilde{\theta}_\tau = 0 \quad (23)$$

and the BCs become

$$\tilde{\varphi}(0,\tau) = 0, \quad \tilde{\varphi}_\eta(0,\tau) = 0, \quad \tilde{\theta}(0,\tau) = 0 \quad (24.1)$$

$$\tilde{\varphi}_\eta(\eta,\tau) \to 0, \quad \tilde{\theta}(\eta,\tau) \to 0 \text{ as } \eta \to \infty \quad (24.2)$$

Now we take $\tau = 0$ to test stability of the dual solutions for the steady state and set $\tilde{\varphi}(\eta,0) = \tilde{\varphi}_0$ and $\tilde{\theta}(\eta,0) = \tilde{\theta}_0$. Therefore Eqs. (22) and (23) reduce to

$$\tilde{\varphi}_0''' + \varphi_0\tilde{\varphi}_0'' + \varphi_0''\tilde{\varphi}_0 - (2\varphi_0' + M^2 - \beta)\tilde{\varphi}_0' = 0 \quad (25)$$

$$\tilde{\theta}_0'' + \Pr(\varphi_0\tilde{\theta}_0' + \theta_0'\tilde{\varphi}_0 + \beta\tilde{\theta}_0) = 0 \quad (26)$$

The BCs are

$$\tilde{\varphi}_0(0) = 0, \quad \tilde{\varphi}_0'(0) = 0, \quad \tilde{\theta}_0(0) = 0 \quad (27.1)$$

$$\tilde{\varphi}_0'(\eta) \to 0, \quad \tilde{\theta}_0(\eta) \to 0 \text{as} \eta \to \infty \quad (27.2)$$

Clearly Eqs. (25) and (26) are linear and homogeneous and also the boundary conditions (27.1) and (27.2) are homogeneous. There is no loss of generality to assume $\tilde{\varphi}_0'' = 1$. Also the above equations constitute an eigenvalue problem where β is the eigenvalue and gives a set of infinite number of eigenvalues in descending order like $\beta_1 \le \beta_2 \le \beta_3 \cdots\cdots$. The sign of β_i's (for $i = 2, 3, 4, \cdots$) follow the sign of β_1. If the smallest eigenvalue $\beta_1 > 0$, the solution is stable, otherwise unstable. Note that Eq. (9) is independent of θ, so if the solutions of (9) is stable then it is true for the solutions of (10) also. Therefore we solve Eq. (25) with the boundary conditions (27.1) and $\tilde{\varphi}_0'' = 1$ using the numerical values of Eq. (9). The smallest eigenvalue β_1 is determined with the shooting algorithm and Newton method so that the third boundary condition $\tilde{\varphi}_0'(\eta) \to 0$ as $\eta \to \infty$ (Following the method of Cebeci and Keller [13]).

V. RESULTS AND DISCUSSIONS

Figs. (3) and (4) show the variations of $\varphi''(0)$ and $-\theta'(0)$ with λ. Negative values of λ correspond to surface shrinking and $\lambda > 0$ stands for surface stretching. Our computations reveal that dual solutions exist for the above free BVP. It is noticed that we get unique solution for stretching sheet case while for shrinking sheet, we obtain dual solutions and the values of critical pointλ_c are given in Figs. (3) and (4). Our numerical results show that for $M = 0$, dual solution exist in the range $-1.24657 \le \lambda \le -1$, which agrees with the reported results of Wang [7] and Bhattacharyya [8]. It is found that for $M = 0.1$, the dual solution branches exist within the range $-1.25537 \le \lambda \le -1.075$ while for $M = 0.2$, the range of the dual solution branches is $-1.28181 \le \lambda \le -1.1648$. From these novel results, it can be confirmed that, the increment of Hartmann number (M) increases the absolute value of theλ_c . Figs. (5) and (6) elucidate the stream lines for $M = 0.2$ and $\lambda = -1.24$ for upper and lower branches respectively.

Figs.(7) and (8) depict the dual profiles of $\varphi'(\eta)$ and θ(η) for several values of Hartmann number (M) at $\lambda = -1.24$ and $Pr = 1$. Fig. (7) elucidates that the effect of increasing M, increases $\varphi'(\eta)$ in the upper branch (UB). But the opposite trend is found in the lower branch (LB). Fig.(8) also elucidates that the increment of M diminishes the temperature profiles $\theta'(\eta)$ in the UB, but the opposite trend is found in the LB. Figs.(9) and (10) depict the dual profiles of the velocity and temperature for several λ at $M = 0.1$ and $Pr = 1$. Fig. (9) elucidates that the velocity profile $\varphi'(\eta)$ decreases in the UB with increasing in $|\lambda|$, but the opposite trend is observed in the LB. Fig. (10) elucidates that the temperature profile $\theta'(\eta)$ increases in the UB with increasing in $|\lambda|$ where for LB, it decreases. The boundary layer thickness for the USB is lower than the LSB for these figures. Similar trend was found in the reported results of Bhattacharyya [8] for $M = 0$.

The plot of the smallest eigenvalue β_1 with the shrinking parameter λ is depicted in Fig. (11) for$M = 0.1$. It is clear from this figure that all the $\beta_1 > 0$ in the USB and $\beta_1 < 0$ in the LSB. Hence the USB is the only stable solution.

VI. CONCLUSIONS

The present study emphasizes the numerical solutions and the stability analysis of the dual solutions of this model. In addition the heat transfer is also discussed in this study. The resulting nonlinear and coupled self-similar equations are integrated with the aid of shooting method. We have seen that unique solution exist for all $\lambda > 0$, while dual solutions exist in the particular range of shrinking rate λ. One of the new findings of our study is the magnitude of the critical value λ_c increases with the increasing of Hartmann number, M. Moreover, it is observed that the boundary layer thickness for the USB is thinner than the LSB. A linear stability analysis is conducted by adopting the method of Merkin [12] and the lowest eigenvalues are obtained numerically employing the method of Cebeci and Keller [13]. Our numerical results reveal that the lower branch is unstable while the upper branch is stable and physically meaningful.

ACKNOWLEDGEMENTS

The first author thankful to the Ministry of Human Research Development (MHRD) Govt. of India, and the NIT Rourkela for providing financial assistance for carrying out this work.

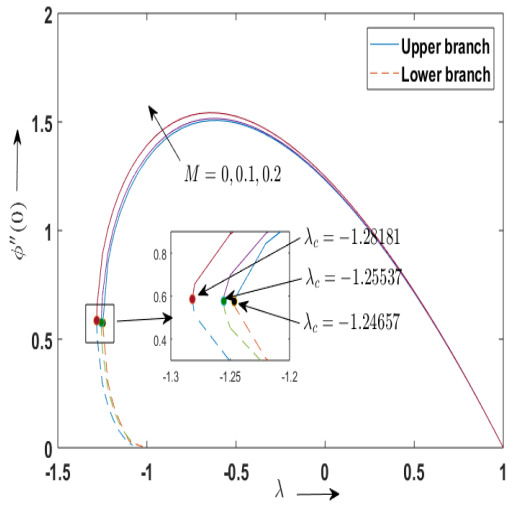

Fig. 3. Variation of $\varphi''(0)$ with λ for several M.

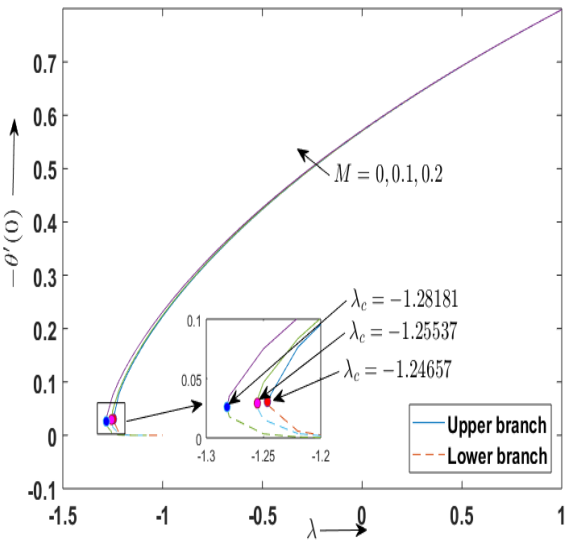

Fig. 4. Variation of $-\theta'(0)$ with λ for several M at $Pr = 1$.

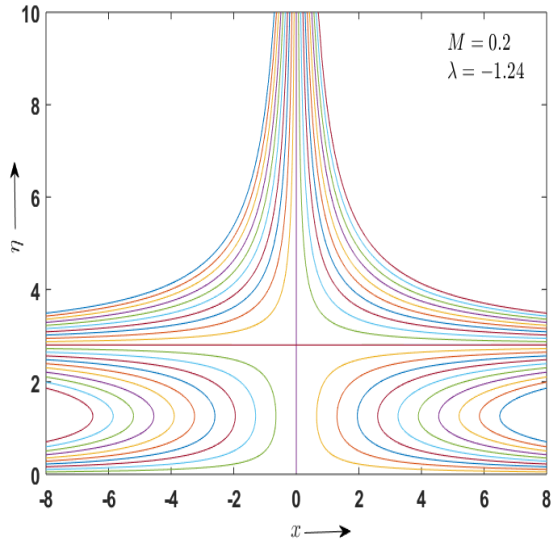

Fig. 5. Stream function for upper branch for $M = 0.2$ and $\lambda = -1.24$.

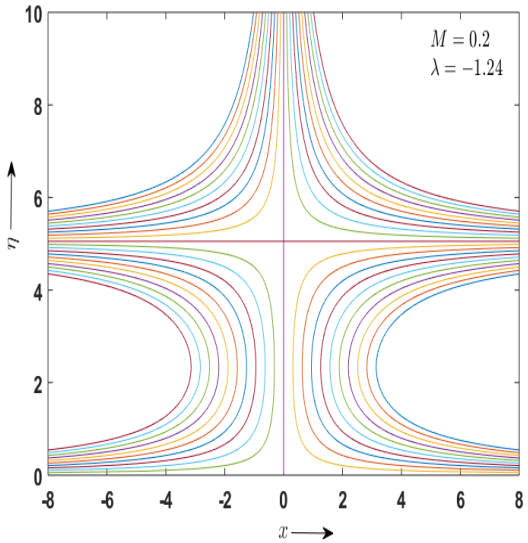

Fig. 6. Stream function for lower branch for $M = 0.2$ and $\lambda = -1.24$.

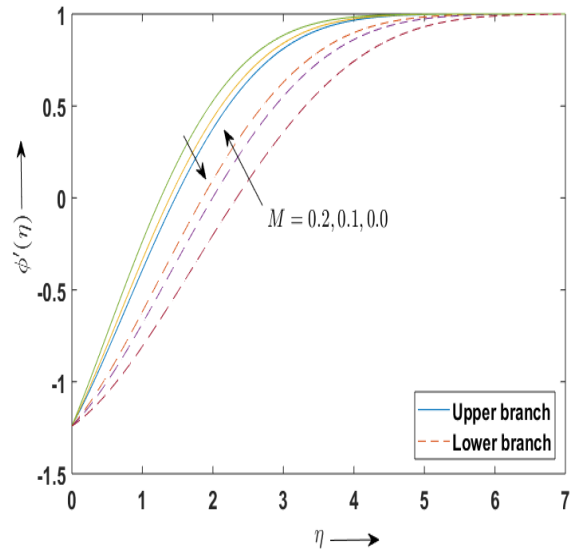

Fig. 7. Variation of dual $\varphi'(\eta)$ with η for several M at $\lambda = -1.24$.

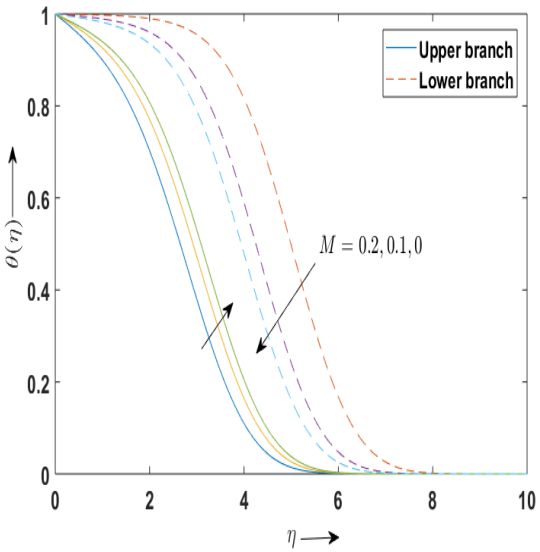

Fig. 8. Variation of dual $\theta(\eta)$ with η for several M at $\lambda = -1.24$ and $Pr = 1$.

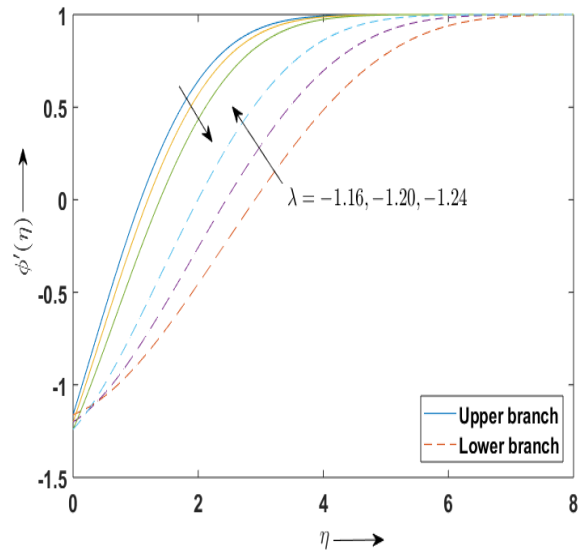

Fig. 9. Variation of dual $\varphi'(\eta)$ with η for several λ at $M = 0.1$.

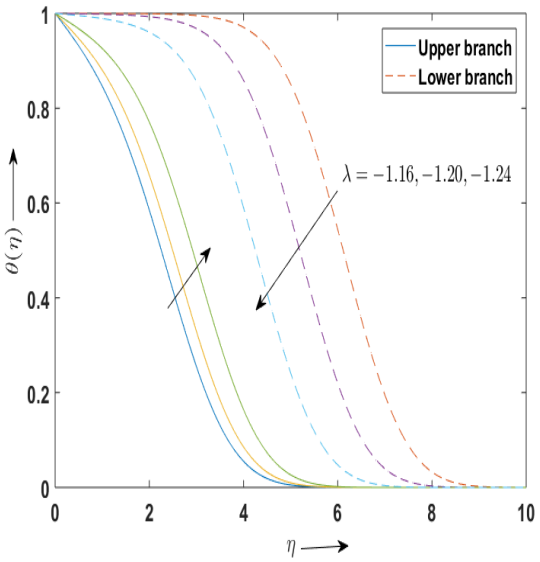

Fig. 10. Variation of dual $\theta(\eta)$ with η for several λ at $M = 0.1$ and $Pr = 1$.

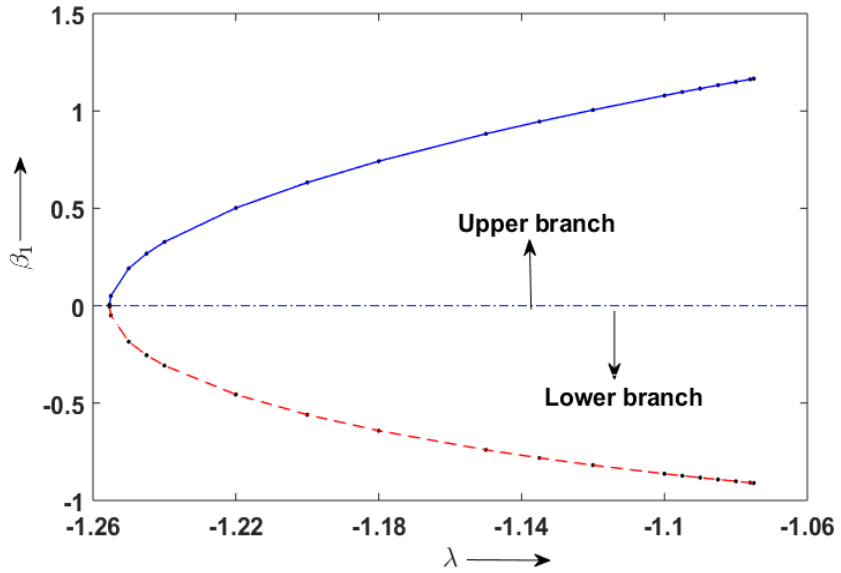

Fig. 11. Plot of the smallest eigenvalue β_1 with λ at $M = 0.1$.

REFERENCE

[1] L. J. Crane, Flow past a stretching sheet, ZeitschriftfürangewandteMathematik und Physik ZAMP, 21(4), 645-647(1970). https://doi.org/10.1007/BF01587695

[2] K. R. Rajagopal, T. Y. Na, A. S. Gupta, Flow of a viscoelastic fluid over a stretching sheet, RheologicaActa, 23(2), 213-215(1984). https://doi.org/10.1007/BF01332078

[3] K. Vajravelu, D. Rollins, Heat transfer in an electrically conducting fluid over a stretching surface, International journal of non-linear mechanics, 27(4), 265-277(1992). https://doi.org/10.1016/0020-7462(92)90085-L

[4] K. Hiemenz, Die Grenzschicht an einem in den gleichformigenFlussigkeitsstromeingetauchtengeradenKreiszylinder, DinglersPolytech. J., 326, 321-324(1911).

[5] T. C. Chiam, Stagnation-point flow towards a stretching plate, Journal of the physical society of Japan, 63(6), 2443-2444(1994). https://doi.org/10.1143/jpsj.63.2443

[6] T. R. Mahapatra, A. S. Gupta, Magnetohydrodynamic stagnation-point flow towards a stretching sheet. ActaMechanica, 152(1-4), 191-196(2001). https://doi.org/10.1007/BF01176953

[7] C. Y. Wang, Stagnation flow towards a shrinking sheet, International Journal of Non-Linear Mechanics, 43(5), 377-382(2008). https://doi.org/10.1016/j.ijnonlinmec.2007.12.021

[8] K. Bhattacharyya, Dual solutions in boundary layer stagnation-point flow and mass transfer with chemical reaction past a stretching/shrinking sheet, International Communications in Heat and Mass Transfer, 38(7), 917-922(2011). https://doi.org/10.1016/j.icheatmasstransfer.2011.04.020

[9] K. Bhattacharyya, S. Mukhopadhyay, G. C. Layek, and I. Pop, Effects of thermal radiation on micropolar fluid flow and heat transfer over a porous shrinking sheet, International Journal of Heat and Mass Transfer, 55(11-12), 2945-2952(2012). https://doi.org/10.1016/j.ijheatmasstransfer.2012.01.051

[10] R. Sharma, R. Ishak, and I. Pop, Stability analysis of magnetohydrodynamic stagnation-point flow toward a stretching/shrinking sheet. Computers & Fluids, 102, 94-98(2014). https://doi.org/10.1016/j.compfluid.2014.06.022

[11] I. S. Awaludin, P. D. Weidman, and A. Ishak,, Stability analysis of stagnation-point flow over a stretching/shrinking sheet, AIP Advances, 6(4), 045308(2016). https://doi.org/10.1063/1.4947130

[12] J. H. Merkin, Mixed convection boundary layer flow on a vertical surface in a saturated porous medium, Journal of Engineering Mathematics, 14(4), 301-313(1980). https://doi.org/10.1007/BF00052913

[13] T. Cebeci, and H. B. Keller, Shooting and parallel shooting methods for solving the Falkner-Skan boundary-layer equation, Journal of Computational Physics, 7(2), 289-300(1971). https://doi.org/10.1016/0021-9991(71)90090-8